Thin-Walled Structures 133 (2018) 216–225

Contents lists available at ScienceDirect

Thin-Walled Structures

journal homepage: www.elsevier.com/locate/tws

Full length article

Tailoring the optimal load-carrying efficiency of hierarchical stiffened shells by competitive sampling

Kuo Tian[a], Bo Wang[a,*], Ke Zhang[a], Jiaxin Zhang[b], Peng Hao[a], Ying Wu[c]

[a] Department of Engineering Mechanics, State Key Laboratory of Structural Analysis for Industrial Equipment, Dalian University of Technology, Dalian 116024, China
[b] Department of Civil Engineering, Johns Hopkins University, Baltimore, MD 21218, USA
[c] Department of Astronautic Science and Mechanics, Harbin Institute of Technology, Harbin 150001, China

ARTICLE INFO

Keywords:
Shell buckling
Hierarchical stiffened shell
Surrogate-based optimization
Asymptotic homogenization method
Competitive sampling

ABSTRACT

The hierarchical stiffened shell is a promising aerospace structure configuration with high load-carrying capacity, however, it is challenging to fully explore its optimal load-carrying efficiency. Therefore, a bi-level optimization framework is proposed for hierarchical stiffened shells. In the first level of the optimization framework, a parallel computing numerical-based smeared stiffener method (NSSM) is first introduced for the fast prediction of critical buckling load and mode, by combining the numerical implementation of asymptotic homogenization (NIAH) method with the Rayleigh-Ritz method. Then, a large-scale Latin hypercube sampling (LHS) is performed in the entire design space based on NSSM, and a set of competitive sampling points is collected from the Pareto front of LHS results according to a screening criterion of load-carrying efficiency. In the second level, a surrogate-based optimization using radial basis function (RBF) technique is performed based on generated competitive sampling points with high load-carrying efficiency. Finally, detailed comparisons between optimal results of the proposed optimization method based on the competitive sampling method and the traditional surrogate-based optimization method based on the RBF technique and the LHS sampling method are made from the viewpoint of computational efficiency and global optimizing ability. Spending an approximate computational time, the optimal buckling result of the proposed method increases by 23.7% than that of the traditional method. In order to achieve an approximate global optimization result, the proposed method is able to reduce the computational time by 74.4% than the traditional method. By evaluating competitive sampling results, it can also be concluded that the partial global buckling mode and global buckling mode are most dominant buckling modes for hierarchical stiffened shells with the thick skin and closely-spaced stiffeners, which are prone to obtain a higher load-carrying efficiency.

1. Introduction

Owing to the high specific strength and stiffness, stiffened shells have been widely used in aerospace engineering [1,2]. Under the axial compression loading condition, buckling is the major failure mode for stiffened shells. In order to improve the load-carrying capacity of stiffened shells, diverse stiffener patterns have been developed [3–8], including isogrid stiffeners, curvilinear stiffeners, orthogrid stiffeners, Kagome stiffeners, Omega stiffeners, etc. Another promising stiffener pattern is hierarchical stiffeners, which are composed of major stiffeners (in larger stiffener size) and minor stiffeners (in smaller stiffener size). Based on numerical and experimental methods, Quinn et al. [9–11] and Houston et al. [12] studied the excellent mechanical performance of hierarchical stiffened panels by comparison against traditional stiffened panels with the same weight. The low imperfection sensitivity of hierarchical stiffened shells was verified by Wang et al. [13], which indicates that the hierarchical stiffened shell is a more robust and safe design against imperfections than the traditional stiffened shell. Taking the imperfection sensitivity into consideration, Hao et al. [14] proposed an efficient hybrid optimization framework for hierarchical stiffened shells based on smeared stiffener method and finite element method. Inspired by the dragonfly wing, Wang et al. [15] developed a novel hierarchical stiffened shell reinforced by mixed stiffener patterns (composed of orthogrid major stiffeners and triangle minor stiffeners), which significantly expands the design space of hierarchical stiffened shells. Aiming at obtaining the optimal buckling load, Zhao et al. [16] performed optimizations for hierarchical stiffened shells based on linear buckling and nonlinear collapse analyses respectively. In order to improve the analysis efficiency of hierarchical stiffened plates and shells, Wang et al. [17,18] established an

* Corresponding author.
E-mail address: wangbo@mail.dlut.edu.cn (B. Wang).

https://doi.org/10.1016/j.tws.2018.03.029
Received 7 December 2017; Received in revised form 14 February 2018; Accepted 27 March 2018
Available online 05 October 2018
0263-8231/

equivalent model to accelerate the buckling analysis and optimization. In addition, the blast-resistant capacity and thermal buckling capacity of hierarchical stiffened structures were investigated in Refs. [19,20]. Up to now, the hierarchical stiffened shell is still a theoretical concept. But currently it is being evaluated and designed for new-generation heavy lift launch vehicles.

Typical buckling analysis methods for stiffened shells and hierarchical stiffened shells can be mainly summarized as finite element method (FEM), smeared stiffener method (SSM) and hybrid model method. Rahimi et al. [21] used the eigenvalue buckling method in ANSYS software to analyze the effect of stiffener profile on linear buckling load in composite isogrid stiffened shell under axial loading. Wang et al. [17] performed the linear buckling analysis on hierarchical stiffened panels based on the Lanczos method. Aiming at capturing the nonlinear post-buckling path of stiffened shells, the explicit dynamics method is employed for the detailed FE analysis of stiffened shells [22] and hierarchical stiffened shells [13,14,15,18], showing a good agreement with experimental results [23,24]. SSM is based on an analytical method to smear the skin and stiffeners into an equivalent lamina, and then the equivalent stiffness coefficients are substituted into the Rayleigh-Ritz method to calculate the buckling load [25,26]. SSM has been used in the analysis and optimization of stiffened shells, indicating higher computational time-consuming efficiency than a detailed FEM model [27–31]. However, Wang et al. [32] pointed out that SSM is not accurate enough because the coupling stiffness cannot be obtained accurately in SSM. In comparison to the analytical equivalent method in SSM, the numerical-based Asymptotic Homogenization Method (AHM) shows higher prediction accuracy because of its rigorous mathematical foundation of perturbation theory [33]. By combining the AHM with the Rayleigh-Ritz method, a numerical-based smeared stiffener method (NSSM) was proposed for stiffened composite cylindrical shells [32]. Its high prediction accuracy has been validated for diverse stiffener patterns by comparison against the traditional SSM [32]. Due to the fact that SSM cannot consider the nonlinear post-buckling capacity of stiffened shells, Tian et al. [34] and Hao et al. [35–37] established an effective hybrid model by combining equivalent methods with the detailed FE analysis method for stiffened shells and hierarchical stiffened shells. Its core idea is to first calculate equivalent stiffness coefficients based on equivalent methods, and then assign them into stiffness properties in the finite element model. After the establishment of the equivalent unstiffened shell, the explicit dynamics method is used to calculate the collapse load. Remarkably, the hybrid model developed by Tian et al. [34] reduced the post-buckling analysis time of stiffened shells by 92% by comparison against the detailed FEM model. As one kind of thin-walled structures, stiffened shells are sensitive to imperfections. In the early stage, the NASA SP-8007 guideline [38] is used to predict the lower-bound buckling load for shell structures. As demonstrated by many experimental studies [24,39], NASA SP-8007 is overly conservative, resulting in excess structural weight. Many research groups are developing advanced, accurate and realistic imperfection analysis methods. One representative work is the Shell Buckling Knockdown Factor (SBKF) project by NASA, which developed, analyzed and validated new design criteria for grid stiffened shells [40,41]. Another outstanding work is the single boundary perturbation approach (SBPA) proposed by Wagner et al. [42–47] in German Aerospace Center. The SBPA can induce a physical meaningful and realistic buckling response in a cylindrical shell. The significant effectiveness and efficiency of SBPA have been extensively verified and validated for unstiffened cylindrical shells, stiffened cylindrical shells and unstiffened conical shells [42–47], which can be regarded as a promising and advanced prediction method of the knockdown factor (KDF) value for shell structures. Based on optimization techniques, the Worst Multiple Perturbation Load Approach (WMPLA) was proposed and developed by Wang et al. [48]. It uses a finite number of single dimple-shape imperfections to cover the realistic imperfection in practice. After optimizing the amplitude and location of the combination of multiple perturbation loads, the lower-bound buckling load can be determined. The effectiveness of WMPLA was validated by a full-scale buckling test of isogrid stiffened shells [23].

For the purpose of achieving a higher buckling load or a lighter structural weight, many efforts have been made for the design and optimization of stiffened shells and hierarchical stiffened shells. Major optimization variables for stiffened shells include the stiffener height, the stiffener thickness, the skin thickness and numbers of stiffeners along axial and circumferential directions [49]. Extra optimization variables for hierarchical stiffened shells are major and minor stiffener heights, major and minor stiffener thicknesses, and numbers of major and minor stiffeners along axial and circumferential directions [17,28]. In order to search out the global optimal result, heuristic optimization algorithms are good choices (for examples, Genetic Algorithm [50,51], ant colony optimization algorithm [52], particle swarm optimization algorithm [53,54] and Shuffled Frog-Leaping Algorithm [55]). It should be pointed out that, heuristic optimization algorithms need large-scale iterations, and thus analytical buckling analysis method is combined with heuristic optimization algorithms in most instances [50–55]. When solving the large-scale optimization problem based on detailed finite element method, the surrogate modeling approach is an efficient solution to accelerate the optimization process. Lene et al. [56] used response surfaces methodology (RSM) for the surrogate-based optimization of a composite stiffened cylinder. According to literatures [13–16], the traditional optimization method for hierarchical stiffened shells is the conventional surrogate-based optimization method based on the RBF technique and the LHS sampling method. Zhao et al. [16] proposed a surrogate-based optimization framework for hierarchical stiffened shells based on radial basis function (RBF) surrogate modeling technology, and the optimal hierarchical grid design contributed to avoiding the undesired local buckling. Furthermore, the hybrid model was integrated into the surrogate-based optimization framework to replace the detailed finite element model [15,17], which significantly improved the optimization time-consuming efficiency of hierarchical stiffened shells. According to the physical and geometric characteristics of the design parameters involved in the complicated optimization process of stiffened shells with a large number of variables, many authors proposed efficient multilevel or multistep optimization strategies to search for the optimum design [57]. Liu et al. [58] applied a bi-level strategy to the post-buckling optimization of composite stiffened panels, by dividing the optimization process into the laminate level and the panel level. The optimization objective of the panel level optimization is to minimize the structural weight by optimizing the cross-sectional geometry, and that of the laminate level optimization is to seek optimum stacking sequences satisfying laminate design rules. Considering the multi-scale features of nano-enhanced composite structures, Dormohammadi et al. [59] decomposed the complex optimization problem into three levels, including a macroscale structural optimization, a macro-scale material optimization and a micro-scale material optimization. Wang et al. [18] established a multilevel optimization framework by decomposing the entire optimization into a major-level sub-optimization and a minor-level sub-optimization, where the Fixed-Point Iteration method is integrated to accelerate the convergence of the optimization framework.

This paper is organized as follows. First, the formulae of NSSM are derived for the critical buckling analysis of hierarchical stiffened shells. Meanwhile, the parallel computing method is integrated into NSSM, which can further improve the prediction efficiency of NSSM. Then, a bi-level optimization framework is established. In the first level, a large-scale Latin hypercube sampling (LHS) is performed among the entire design space based on NSSM, in order to generate a Pareto front set according to a screening criterion of load-carrying efficiency. In the second level, the surrogate-based optimization is performed based on the generated set of competitive sampling points with high load-carrying efficiency. Finally, detailed comparisons between optimal results of the proposed method and traditional optimization methods are made

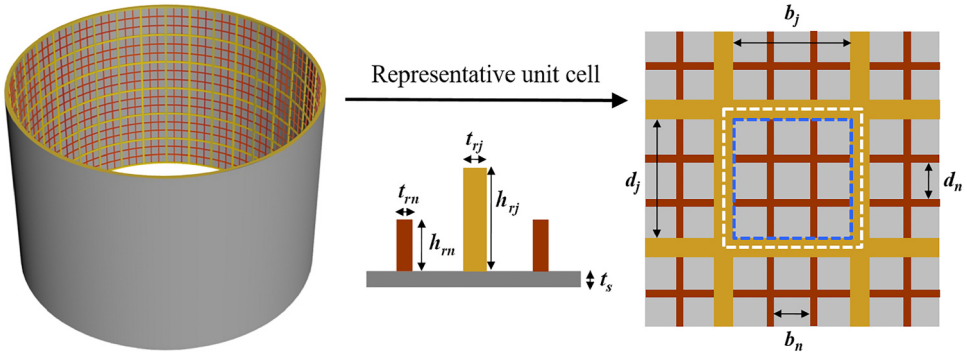

Fig. 1. Schematic diagrams of the hierarchical stiffened shell and the representative unit cell. (For interpretation of the references to color in this figure, the reader is referred to the web version of this article.)

from the viewpoint of computational efficiency, global optimizing ability and imperfection sensitivity.

2. Methodology

2.1. A brief introduction of NIAH method

NIAH is more competitive in calculation efficiency and operability, by comparison against the traditional numerical implementation method of AHM based on numerous integral operations. Formula derivations of NIAH method involved in this paper totally follow the research work by Cai et al. [33]. In order to keep simple, detailed formula derivations are omitted and only the steps of numerical implementation are summarized briefly as follows:

Step 1: A representative unit cell is divided out of the stiffened shell, and its FEM model is built in the commercial finite element software with detailed model information. Then, the unit nodal displacement fields χ_i^0 and $\bar{\chi}_i^0$ are applied to the unit cell model. Where subscripts i and j denote load cases ($i, j \in \{1, 2, 6\}$). The variables with an overline represent the flexural variables, while the others are in-plane variables. The first FEM static analysis is run, and the nodal force vectors $\mathbf{f}_i$ and $\bar{\mathbf{f}}_i$ are outputted.

Step 2: The above force vectors are then applied to each node of the original FEM model, and periodic boundary conditions are set up. By driving the second FEM static analysis, characteristic nodal displacements $\mathbf{a}_i^*$ and $\bar{\mathbf{a}}_i^*$ are obtained directly.

Step 3: Above characteristic nodal displacement fields $\mathbf{a}_i^*$ and $\bar{\mathbf{a}}_i^*$ are applied to corresponding nodes of the original FEM model, and then the third FEM static analysis is performed to calculate the characteristic nodal reaction forces $\mathbf{P}_i^*$ and $\bar{\mathbf{P}}_i^*$.

Step 4: As Eq. (1) shows, the extensional stiffness coefficients A_{ij}, coupling stiffness coefficients B_{ij}, and bending stiffness coefficients D_{ij} of the periodic unit cell Ω can be obtained directly by the dot product operation of unit nodal displacement vectors, nodal force vectors, characteristic nodal displacements vectors and characteristic nodal force vectors.

$$
\begin{aligned}
A_{ij} &= \frac{1}{|\Omega|}(\chi_i^0 - \mathbf{a}_i^*)^{\mathrm{T}}(\mathbf{f}_j - \mathbf{P}_j^*)\\
B_{ij} &= \frac{1}{|\Omega|}(\chi_i^0 - \mathbf{a}_i^*)^{\mathrm{T}}(\bar{\mathbf{f}}_j - \bar{\mathbf{P}}_j^*)\\
D_{ij} &= \frac{1}{|\Omega|}(\bar{\chi}_i^0 - \bar{\mathbf{a}}_i^*)^{\mathrm{T}}(\bar{\mathbf{f}}_j - \bar{\mathbf{P}}_j^*)
\end{aligned}
\tag{1}
$$

By means of above four steps, a unit cell of the stiffened shell can be easily equivalent to stiffness coefficients A_{ij}, B_{ij} and D_{ij} by operation of the commercial software.

2.2. Parallel computing NSSM for hierarchical stiffened shells

Based on the NIAH method, Wang et al. [32] proposed a Numerical-based Smeared Stiffener Method (NSSM) for traditional stiffened shells, which is a more efficient linear buckling analysis method than FEM. Its steps are as follows: Firstly, a representative unit cell is divided out of the stiffened shell. Secondly, the equivalent stiffness coefficients A_{ij}, B_{ij} and D_{ij} of the unit cell are calculated based on NIAH. Finally, by substituting above coefficients into the formula of Rayleigh-Ritz method, the linear buckling load of stiffened shells can be easily obtained. It should be pointed out that NSSM is only suitable for capturing the global buckling load of traditional stiffened shells. However, due to the increase of structural hierarchy, multiple buckling modes are likely to occur in the hierarchical stiffened shells, including the global buckling mode, partial global buckling mode and local buckling mode [13]. Thus, it is necessary to make a supplement for NSSM, and then it will be chosen as the rapid equivalent evaluation method for multiple buckling modes of hierarchical stiffened shells in this paper.

As shown in Fig. 1, the region surrounded by the white dot line is the representative unit cell (RUC) of global buckling mode, which is composed of the skin, the minor stiffeners and the half of the major stiffeners. Where, b_j and d_j represent the widths of adjacent axial and circumferential major stiffeners, b_n and d_n represent the widths of adjacent axial and circumferential minor stiffeners, h_{rj} and h_{rn} represent the heights of major and minor stiffeners, t_{rj} and t_{rn} represent the thickness of major and minor stiffeners. Following the steps of NSSM, the stiffness coefficients A_{ij}^g, B_{ij}^g and D_{ij}^g of the unit cell of global buckling mode are obtained by means of the NIAH method. Based on these stiffness coefficients, Rayleigh-Ritz method is used to calculate the linear buckling load. Firstly, we suppose the displacement components of the hierarchical stiffened shells as three double Fourier series according to the buckling mode shapes,

$$
\begin{aligned}
u &= \sum_{m=1}^{\infty}\sum_{n=1}^{\infty} a_{mn}\cos(m\alpha\, x)\sin(n\beta\, y)\\
v &= \sum_{m=1}^{\infty}\sum_{n=1}^{\infty} b_{mn}\sin(m\alpha\, x)\cos(n\beta\, y)\\
w &= \sum_{m=1}^{\infty}\sum_{n=1}^{\infty} c_{mn}\sin(m\alpha\, x)\sin(n\beta\, y)
\end{aligned}
\tag{2}
$$

where $\alpha = \pi/L$, $\beta = 1/\mathrm{R}$, L is the height of hierarchical stiffened shell, and R is the radius of hierarchical stiffened shell, m denotes the number of axial half waves, n denotes the number of circumferential full waves.

Substitute above displacement components into the expressions of total potential energy, then set the first derivative of the total potential energy with respect to a_{mn}, b_{mn}, and c_{mn} to be zero, and finally obtain the linear global buckling load P_g,

$$P_g = \frac{2R}{\pi}\left(\frac{L}{m}\right)^2 \frac{\begin{vmatrix} K_{11} & K_{12} & K_{13} \\ K_{21} & K_{22} & K_{23} \\ K_{31} & K_{32} & K_{33} \end{vmatrix}}{\begin{vmatrix} K_{11} & K_{12} \\ K_{21} & K_{22} \end{vmatrix}} \tag{3}$$

$$K_{11} = A_{11}^g\left(\frac{m\pi}{L}\right)^2 + A_{66}^g\left(\frac{n}{R}\right)^2 - 2A_{16}^g\left(\frac{m\pi}{L}\right)\left(\frac{n}{R}\right) \tag{4}$$

$$K_{22} = A_{22}^g\left(\frac{n}{R}\right)^2 + A_{66}^g\left(\frac{m\pi}{L}\right)^2 - 2A_{26}^g\left(\frac{m\pi}{L}\right)\left(\frac{n}{R}\right) \tag{5}$$

$$K_{33} = 2(D_{12}^g + 2D_{66}^g)\left(\frac{m\pi}{L}\right)^2\left(\frac{n}{R}\right)^2 + D_{11}^g\left(\frac{m\pi}{L}\right)^4 + D_{22}^g\left(\frac{n}{R}\right)^4 - 4D_{16}^g\left(\frac{m\pi}{L}\right)^3\left(\frac{n}{R}\right) - 4D_{26}^g\left(\frac{m\pi}{L}\right)\left(\frac{n}{R}\right)^3 \tag{6}$$

$$K_{12} = K_{21} = (A_{12}^g + A_{66}^g)\left(\frac{m\pi}{L}\right)\left(\frac{n}{R}\right) - A_{16}^g\left(\frac{m\pi}{L}\right)^2 - A_{26}^g\left(\frac{n}{R}\right)^2 \tag{7}$$

$$K_{13} = K_{31} = -B_{11}^g\left(\frac{m\pi}{L}\right)^3 - (B_{12}^g + 2B_{66}^g)\left(\frac{m\pi}{L}\right)\left(\frac{n}{R}\right)^2 + 3B_{16}^g\left(\frac{m\pi}{L}\right)^2\left(\frac{n}{R}\right) + B_{26}^g\left(\frac{n}{R}\right)^3 \tag{8}$$

$$K_{23} = K_{32} = -B_{22}^g\left(\frac{n}{R}\right)^3 - (B_{12}^g + 2B_{66}^g)\left(\frac{m\pi}{L}\right)^2\left(\frac{n}{R}\right) + B_{16}^g\left(\frac{m\pi}{L}\right)^3 + 3B_{26}^g\left(\frac{m\pi}{L}\right)\left(\frac{n}{R}\right)^2 \tag{9}$$

As a special buckling mode for hierarchical stiffened shells, the partial global buckling mode occurs between the adjacent major stiffeners. In some sense, it can be considered as the local buckling mode between adjacent major stiffeners. As marked in Fig. 1, the unit cell region of partial global buckling mode is surrounded by the blue dot line. Based on the NIAH method, the stiffness coefficients A_{ij}^p, B_{ij}^p and D_{ij}^p of the unit cell of partial global buckling mode can be easily calculated, and then they are substituted into the formula of local buckling load, which was developed by Shi et al. [60]. Thus, the formula of the partial global buckling load P_p can be expressed as follows,

$$P_p = 2\pi R\cdot\pi^2\left[D_{11}^p\left(\frac{m}{b_j}\right)^4 + 2(D_{12}^p + 2D_{66}^p)\left(\frac{mn}{b_j\cdot d_j}\right)^2 + D_{22}^p\left(\frac{n}{d_j}\right)^4\right]\cdot\left(\frac{d_j}{n}\right)^2\cdot P_g \tag{10}$$

It should be noted that, the above methods can be used for hierarchical stiffened shells consist of orthotropic or isotropic materials. It can be easily implemented by assigning orthotropic or isotropic material properties into the RUC model. Then, the formulae for predicting local buckling loads of skin and stiffener are derived for hierarchical stiffened shells.

If the skin and stiffener are both made up of orthotropic materials such as laminates, the stiffness coefficients can be derived based on lamination theory [61],

$$\begin{aligned} A_{ij} &= \sum_{k=1}^{n}(\overline{Q}_{ij})_k(z_k - z_{k-1}) \\ B_{ij} &= \frac{1}{2}\sum_{k=1}^{n}(\overline{Q}_{ij})_k(z_k^2 - z_{k-1}^2) \\ D_{ij} &= \frac{1}{3}\sum_{k=1}^{n}(\overline{Q}_{ij})_k(z_k^3 - z_{k-1}^3) \end{aligned} \tag{11}$$

where k is the index of ply number in one laminate, Q_{ij} is the transformed reduced stiffness of laminate, and z is the coordinate of laminate in thickness.

If the material of the skin and stiffener is isotropic, the above formulation can be simplified as,

$$\begin{aligned} &A_{11} = A_{22} = \frac{Et}{1-\nu^2}, \qquad A_{12} = \frac{\nu Et}{1-\nu^2}, \qquad A_{16} = A_{26} = 0, \\ &A_{66} = \frac{Et}{2(1+\nu)} \\ &B_{ij} = 0 \\ &D_{11} = D_{22} = \frac{Et^3}{12(1-\nu^2)}, \qquad D_{12} = \frac{\nu Et^3}{12(1-\nu^2)}, \\ &D_{16} = D_{26} = 0, \qquad D_{66} = \frac{Et^3}{2(1+\nu)} \end{aligned} \tag{12}$$

where E and ν are Young's modulus and Poisson's ratio of the isotropic material. t is the thickness of the skin or stiffener.

Moreover, as introduced in Ref. [60], the skin local buckling load P_{sl}, the major stiffener local buckling load P_{rjl}, the minor stiffener local buckling load P_{rjn} can be calculated as the following formulae,

$$P_{sl} = 2\pi R\cdot\pi^2\left[D_{11}^{sl}\left(\frac{m}{b_n}\right)^4 + 2(D_{12}^{sl} + 2D_{66}^{sl})\left(\frac{mn}{b_n\cdot d_n}\right)^2 + D_{22}^{sl}\left(\frac{n}{d_n}\right)^4\right]\cdot\left(\frac{d_n}{n}\right)^2\cdot P_g \tag{13}$$

$$P_{rjl} = 2\pi R\cdot\pi^2\left[D_{11}^{rjl}\left(\frac{m}{d_j}\right)^4 + 2(D_{12}^{rjl} + 2D_{66}^{rjl})\left(\frac{mn}{3d_j\cdot h_j}\right)^2 + D_{22}^{rjl}\left(\frac{n}{3h_j}\right)^4\right]\cdot\left(\frac{d_j}{m}\right)^2\cdot P_g \tag{14}$$

$$P_{rnl} = 2\pi R\cdot\pi^2\left[D_{11}^{rnl}\left(\frac{m}{d_n}\right)^4 + 2(D_{12}^{rnl} + 2D_{66}^{rjl})\left(\frac{mn}{3d_n\cdot h_n}\right)^2 + D_{22}^{rnl}\left(\frac{n}{3h_n}\right)^4\right]\cdot\left(\frac{d_n}{m}\right)^2\cdot P_g \tag{15}$$

where superscripts *sl*, *rjl* and *rjn* stand for the variables of skin, major stiffener and minor stiffener respectively.

Finally, the minimum buckling load for above buckling modes is determined as the critical buckling load P_{cr} of the hierarchical stiffened shell, and its corresponding buckling mode is regarded as the critical buckling mode,

$$P_{cr} = \min\{P_g, P_p, P_{sl}, P_{rjl}, P_{rnl}\} \tag{16}$$

In order to obtain the critical buckling load, five calculations need to be carried out with respect to global buckling, partial buckling and local buckling. Due to the fact that these five calculations are independent of each other, the parallel computing method is adopted in this paper to accelerate the five calculations for multiple buckling modes, which is implemented by writing a Batch script to call the five calculations parallelly. In this case, the developed NSSM becomes more efficient for the first-stage design of hierarchical stiffened shells.

Based on the proposed method, the critical buckling load of hierarchical stiffened shells can be quickly calculated (about 6 s) and the critical buckling mode can be explicitly predicted. By contrast, the linear buckling method based on FEM cannot tell users which buckling mode happens explicitly and users must judge the critical buckling mode by itself according to the deformation features. Therefore, this is another advantage of NSSM.

2.3. Bi-level optimization framework based on competitive sampling

A bi-level optimization framework is established according to the flow chart shown in Fig. 2. In the first level, a large-scale LHS (as indicated in [62,63]) is performed in the entire design space based on parallel computing NSSM, and the Pareto front is collected as a set of competitive sampling points according to a screening criterion of load-carrying efficiency. The screening criterion is defined as,

Find: $[\boldsymbol{X}^i]$, $i = 1, 2, \ldots, n$

Such that: $W^i \le W^0$

$$P_{cr}^1 \ge P_{cr}^2 \ge \ldots \ge P_{cr}^i \tag{17}$$

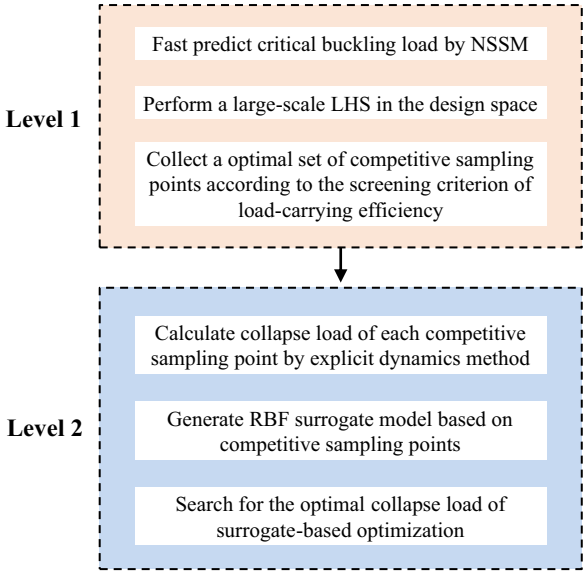

Fig. 2. Flow chart of the bi-level optimization framework for hierarchical stiffened shells.

$$\frac{P_{cr}^{1}}{W^{1}} \geq \frac{P_{cr}^{2}}{W^{2}} \geq \ldots \geq \frac{P_{cr}^{i}}{W^{i}}$$

where, $[\boldsymbol{X}]$ is the set of competitive sampling points, and variables $\boldsymbol{X}$ include the major stiffener height, the major stiffener thickness, the minor stiffener height, the minor stiffener thickness, the skin thickness, the number of axial major stiffeners, the number of circumferential major stiffeners, the number of axial minor stiffeners between axial major stiffeners and the number of circumferential minor stiffeners between circumferential major stiffeners. n is the number of competitive sampling points. P_{cr} is the critical buckling load predicted by NSSM. W and W° are the structural weight corresponding to competitive sampling points and initial design. The screening criterion is governed by three constraint conditions. The first constraint condition is that the structural weight corresponding to competitive sampling points should be not larger than the initial one, which can improve the possibility of searching out the feasible solution. The second constraint condition is to rank the critical buckling load P_{cr} from largest to smallest, and the third constraint condition is to rank the load-carrying efficiency $\frac{P_{cr}}{W}$ from largest to smallest. In other words, a hierarchical stiffened shell with higher critical buckling load and higher load-carrying efficiency simultaneously is more competitive to be collected into the set of competitive sampling points. In addition, if two hierarchical stiffened shells have same values of critical buckling load, the one with higher load-carrying efficiency is more competitive. If the number of LHS is set as 1000 and the given number n of competitive sampling points is 100, we should truncate 100 points form 1000 LHS points according to the screening criterion, and the optimal 100 points can be regarded as the Pareto front of the feasible design space.

In the second level, the RBF surrogate-based optimization is performed based on generated competitive sampling points with high load-carrying efficiency. Multi-Island genetic algorithm (MIGA) [64] is used for searching for the global optimum in the RBF model. The optimization formulations are as follows,

$$\begin{aligned} &\textit{Find}: X \\ &\textit{Maximize}: P_{co} \\ &\textit{Subject to}: W \leq W^{\circ} \\ &\sigma_{max} \leq \sigma_s \end{aligned} \tag{18}$$

where, P_{co} is the collapse load predicted by the explicit dynamics method, and σ_{max} stands for the maximum stress of the hierarchical stiffened shell when the structure collapses, σ_s stands for the yield stress. The optimization objective is to maximize the collapse load P_{co}, under the constraints that the structural weight W is not larger than the initial value W° and the maximum stress σ_{max} is not larger than the yield stress σ_s.

Table 1
The dimension and material information of the hierarchical stiffened shell.

D [mm]	L [mm]	E [MPa]	υ	σ_s [MPa]	σ_b [MPa]	δ
3000	2000	70,000	0.33	563	630	0.07

3. Illustrative example

3.1. Model description for hierarchical stiffened shells

The hierarchical stiffened shell model is established with identical geometrical parameters and boundary conditions described in Refs. [13–15], as shown in Fig. 1. The diameter D of the hierarchical stiffened shell is 3000 mm, and the length L of the hierarchical stiffened shell is 2000 mm, as shown in Table 1. The geometrical parameters are listed in Table 2. Where, t_s represents the skin thickness, N_{aj} represents the number of axial major stiffeners, N_{an} represents the axial minor stiffeners between axial major stiffeners, N_{cj} represents the number of circumferential major stiffeners, N_{cn} represents the circumferential minor stiffeners between circumferential major stiffeners, h_{rj} and h_{rn} represent the major and minor stiffener heights respectively, t_{rj} and t_{rn} represent the major and minor stiffener thicknesses. The mechanical properties of the material used for the hierarchical stiffened shell are listed in Table 1: Young's modulus $E = 70{,}000$ MPa, Poisson's ratio $\upsilon = 0.33$, yield stress $\sigma_s = 563$ MPa, ultimate stress $\sigma_b = 630$ MPa and elongation $\delta = 0.07$. The structural weight W° of the initial design is 354.6 kg. The boundary condition of the hierarchical stiffened shell is to keep the lower end of the hierarchical stiffened shell clamped and the upper end fixed except the degrees of freedom along the axial direction. A uniform axial load is applied to the upper end of the hierarchical stiffened shell. S4R elements (shell element with 4 nodes and reduced numerical integration) are used for the analysis of the FE model in ABAQUS software. A Python script is written to implement the parametric modeling, automatic calculation and post processing of hierarchical stiffened shell models.

3.2. Optimal result by traditional optimization method

The traditional optimization method used for searching for the optimal buckling load of hierarchical stiffened shells is the conventional surrogate-based optimization method based on the RBF technique and the LHS sampling method, as indicated in Refs. [13–15]. Hao et al. [14] established the RBF surrogate model based on 100 sampling points by LHS, and then performed an optimization for hierarchical stiffened shells (Represented as Optimization I in this paper), with the optimal result listed in Table 2. By comparison against the initial design, the optimal collapse load increases by 15.2%. In this study, a work station with a CPU of Intel Xeon E5–2687w @3.10GHzand 64G RAM is used. The total computational time of the optimization process is 178 h as indicated in Ref. [14], which is too time-consuming for the preliminary design of hierarchical stiffened shells. For this kind of complicated multi-modal optimization problem with nine variables, it is difficult to search out the global optimal solution based on a surrogate model with few sampling points. In order to further explore the optimization potential, more LHS sampling points (200, 300 and 400 sampling points) are generated, and corresponding surrogate-based optimizations are carried out, which are represented as Optimization II, Optimization III and Optimization IV respectively. Corresponding optimal results are shown in Table 2. The surrogate-based optimization method used in this paper is decomposed into inner optimization and outer update.

Table 2
The design spaces and optimal results for optimizations.

	t_s [mm]	t_{rj} [mm]	t_{rn} [mm]	h_j [mm]	h_n [mm]	N_{cj}	N_{cn}	N_{aj}	N_{an}	W [kg]	σ_{max} [MPa]	P_{co} [kN]	CPU time [h]
Initial design	4.0	9.0	9.0	23.0	11.5	6	3	30	2	354.6	568	17,265	–
Lower bound	2.5	3.0	3.0	15.0	6.0	3	1	20	1	–	–	–	–
Upper bound	5.5	12.0	12.0	30.0	15.0	9	4	50	4	355.0	563	–	–
Optimization I [14]	4.2	9.7	7.7	30.0	6.0	4	4	48	1	353.6	503	19,893	178
Optimization II	3.3	10.2	4.4	27.3	14.6	7	2	49	2	355.0	517	21,942	345
Optimization III	4.4	7.1	7.3	30.0	11.8	6	1	49	1	354.0	528	23,972	510
Optimization IV	3.3	9.9	3.0	29.9	14.9	8	2	49	2	355.0	562	24,010	702
Optimization V	4.0	7.6	3.0	30.0	14.6	7	3	50	2	355.0	561	24,606	180

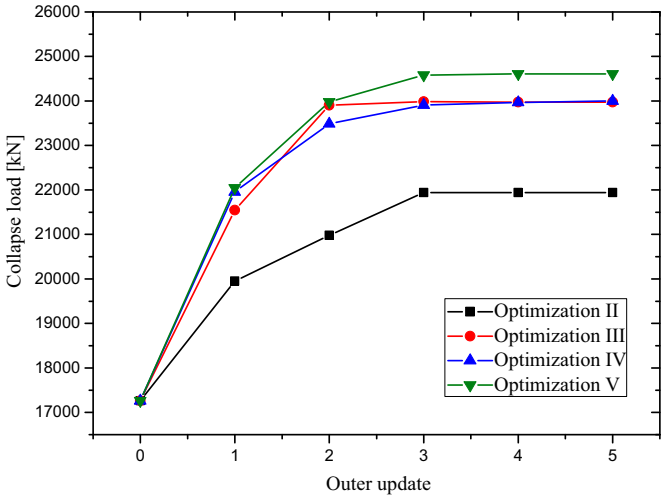

Fig. 3. Iterations of outer updates in surrogate-based optimizations.

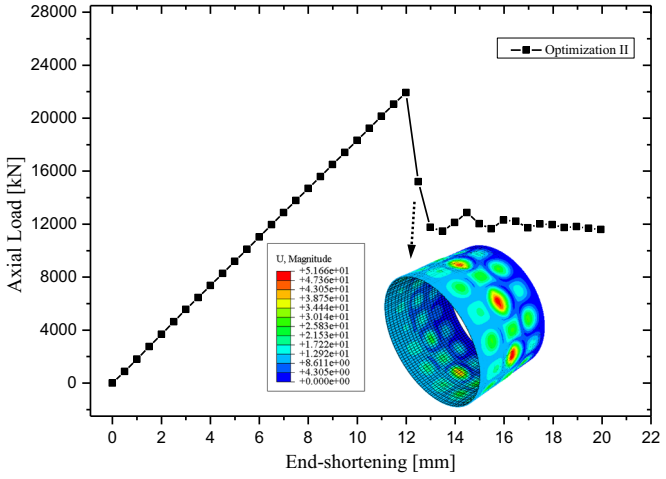

Fig. 4. Load versus end-shortening curve of optimal design of Optimization II.

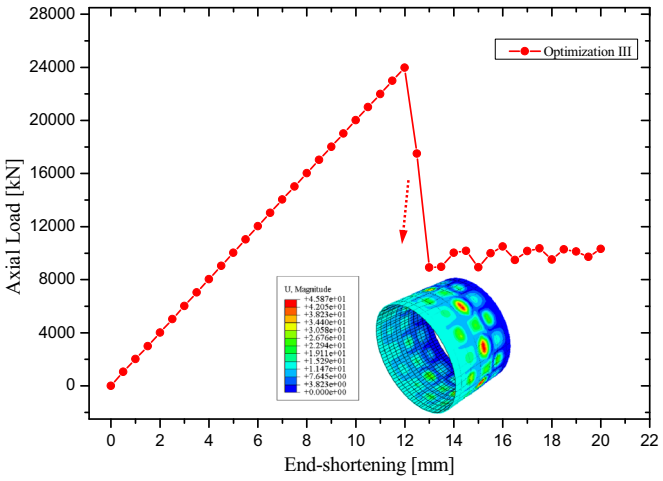

Fig. 5. Load versus end-shortening curve of optimal design of Optimization III.

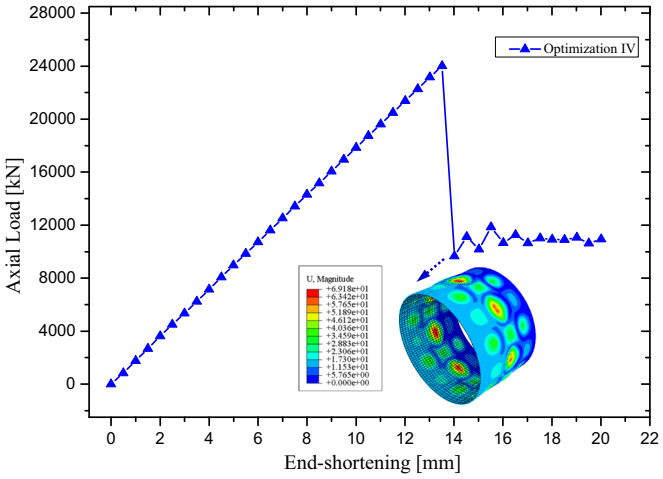

Fig. 6. Load versus end-shortening curve of optimal design of Optimization IV.

Actually, the inner optimization is based on the Multi-Island genetic algorithm (MIGA) technique [64] and needs massive iterations. The optimization is considered to be converged if the relative error between the results obtained from the surrogate model and the ones from exact finite element analysis is small enough, otherwise the surrogate model is updated. If we plot all the details of the inner optimization iterations, it would contain a huge number of points in one figure. For the sake of clarity, iterations based on the surrogate model are removed, and only the history of outer updates is plotted. Iterations of outer updates of Optimization II, Optimization III and Optimization IV are plotted in Fig. 3. Corresponding load versus end-shortening curves of optimal designs of Optimization II, Optimization III and Optimization IV are displayed in Figs. 4, 5 and 6. The optimal collapse load converges to 24,010 kN when the number of sampling points increases to 400. By comparison with the initial design, the converged optimal collapse load increases by 39.1%. Along with the improvement of the global searching ability of the surrogate-based optimization, the total computational time increases sharply from 178 h to 702 h, indicating huge computational cost.

3.3. Optimal result by proposed optimization method

In the first level of the bi-level optimization framework, 5000 LHS points are generated in the entire design space based on the parallel computing NSSM, and the total computational time is 8.3 h. The LHS result is shown in Fig. 7, and a set of optimal 100 design points on the Pareto front is collected according to the screening criterion of load-

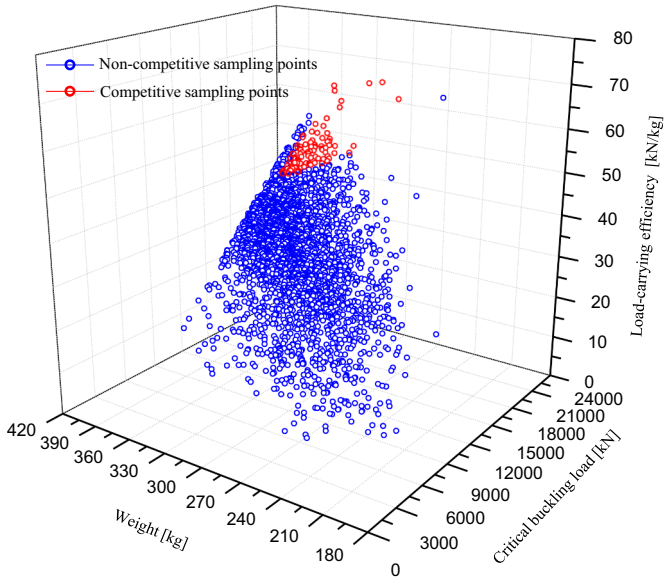

Fig. 7. Latin hypercube sampling result in the first level of the optimization framework. (For interpretation of the references to color in this figure, the reader is referred to the web version of this article.)

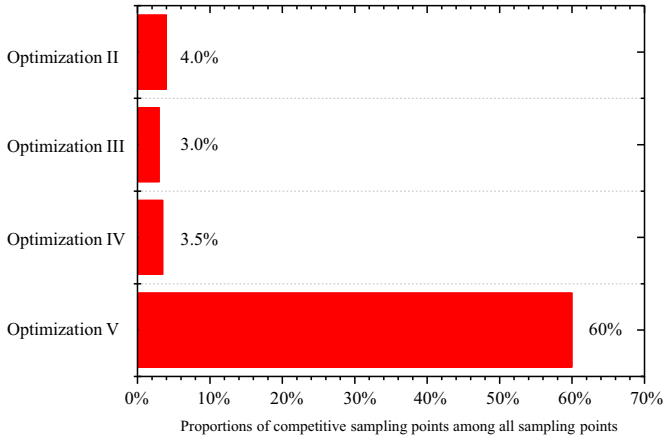

Fig. 8. Proportions of competitive sampling points among all sampling points for optimizations.

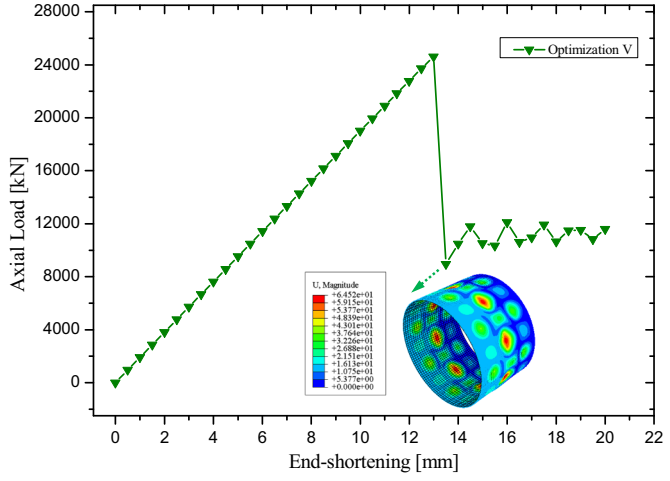

Fig. 9. Load versus end-shortening curve of optimal design of Optimization V.

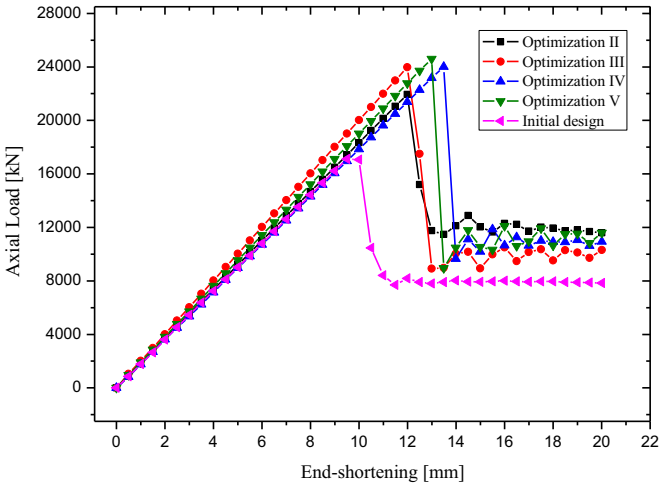

Fig. 10. Load versus end-shortening curve of the initial design and optimal designs.

carrying efficiency, which is marked in red. Then, the explicit dynamics method is performed on these 100 design points to obtain the collapse load value for the corresponding point, and thus their results are used to establish the RBF surrogate model for the next level. Here, we compare proportions of competitive sampling points among all sampling points for the traditional method and the proposed method, as shown in Fig. 8. When a sampling point satisfies the condition that the structural weight is smaller than the initial one, the maximum stress is smaller than the yield stress value and the load-carrying efficiency is larger than the initial one, it is regarded as a competitive sampling point. It can be observed from Fig. 8 that, the proposed method has a significantly higher proportion of competitive sampling points than the traditional LHS sampling method, which means the sampling of the proposed method is more targeted and pointed. In addition, the proportion of competitive sampling points by the traditional LHS sampling method barely increases even though the number of total sampling points increases. Particularly, by evaluating the critical buckling mode of 5000 LHS points, the numbers of design points corresponding to local buckling mode, partial global buckling mode and global buckling mode are 3, 1373 and 3624 respectively. Thus, it can be concluded that the partial global buckling mode and global buckling mode are most dominant for hierarchical stiffened shells with the thick skin and closely-spaced stiffeners.

In the second level, the RBF surrogate model is established based on generated 100 competitive sampling points, which is represented as Optimization V. The surrogate-based optimization is carried out and the optimal result is listed in Table 2. Iterations of outer update of the surrogate-based optimization is shown in Fig. 3. The load versus end-shortening curve of the optimal design of Optimization V is displayed in Fig. 9. By comparison against optimal result (19,893 kN) of the traditional surrogate-based optimization based on 100 sampling points in Table 2, the optimal buckling result (24,606 kN) of the proposed method increases by 23.7% with an approximate computational time, showing an excellent global optimizing ability with limited sampling points of detailed FE models. In order to achieve an approximate global optimal solution as the proposed method, the traditional optimization method is required to generate 400 sampling points of detailed FE models, yet the computational time (702 h) is too time-consuming. It manifests that the proposed method (180 h) can reduce the computational time by 74.4% than the traditional method (702 h). In particular, it should be pointed out that if the parallel computing technique could be used for the sampling process, the total computational time would further decrease. Therefore, the outstanding computational efficiency and global optimizing ability of the proposed method are demonstrated.

Table 3
Effective stiffness coefficients of hierarchical stiffened shells.

	A_{11} [N/mm]	A_{22} [N/mm]	A_{12} [N/mm]	A_{66} [N/mm]	D_{11} [N*mm]	D_{22} [N*mm]	D_{12} [N*mm]	D_{66} [N*mm]
Initial design	406,994	423,422	103,162	106,208	11,667,117	11,998,911	524,995	948,818
Optimization II	408,557	359,884	85,037	87,354	29,037,530	19,868,980	255,689	876,660
Optimization III	454,883	408,835	113,685	116,299	26,684,545	16,354,948	693,509	1,014,496
Optimization IV	396,873	364,524	83,987	86,264	34,875,173	27,056,135	223,487	890,547
Optimization V	427,183	398,034	101,660	104,017	29,255,376	20,317,810	470,504	825,000

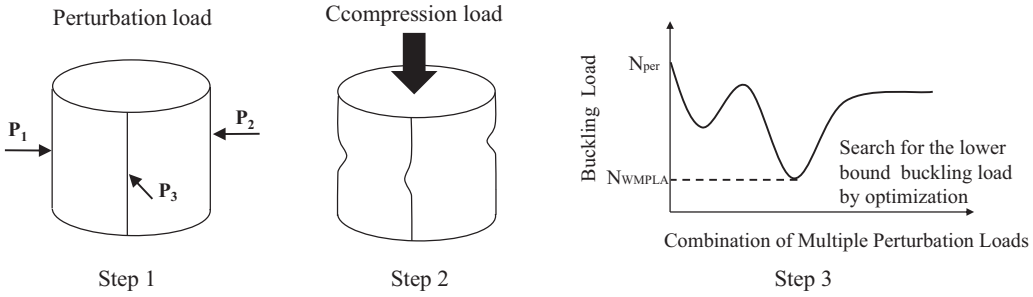

Fig. 11. Flowchart of WMPLA.

Table 4
KDF values of traditional and hierarchical stiffened shells by WMPLA.

	Traditional stiffened shell (Ref. [2])	Hierarchical stiffened shell(Initial design)	Hierarchical stiffened shell (Optimization V)
KDF value	0.63	0.69	0.72

3.4. Discussions on the high buckling load and the low imperfection sensitivity of optimal results

In order to understand the mechanism of the high buckling load of optimal results, a detailed comparison of all load versus end-shortening paths is made for the initial design and optimal designs (Optimization II–V), as shown in Fig. 10. Then, effective extensional and bending stiffness coefficients of these five designs are calculated based on NSSM, as shown in Table 3. It can be concluded from Fig. 10 and Table 3 that, effective extensional and bending stiffness coefficients have a significant influence on the load-carrying capacity of the hierarchical stiffened shell. When the design has higher effective extensional stiffness coefficients, its load versus end-shortening path would have a larger slope of curve, indicating higher axial stiffness of the structure. When the design has higher effective bending stiffness coefficients, it would be more competitive in resisting the onset of the buckling deformation, which would result in a higher collapse load. For the initial design, it has relatively low effective extensional and bending stiffness coefficients. Therefore, its load versus end-shortening path has a small slope of curve and it collapses early. After the optimization, the effective extensional and bending stiffness coefficients increase, and thus the collapse load increases.

Although the optimal design obtained by the proposed optimization framework has a relatively high buckling load, it is very necessary to verify if the optimal design is sensitive to imperfections. Herein, WMPLA is used to evaluate the lower bound of KDF for hierarchical stiffened shells. As described in [13,34], WMPLA can be divided into the following three steps as displayed in Fig. 11. First, multiple lateral perturbation loads (Generally, the number of perturbation loads is set as 3) are applied to the middle of cylinder surface, and the deformation field of the hierarchical stiffened shell is obtained after one static analysis. Second, the above deformation filed is then introduced to the perfect geometry by modifying nodal coordinates, an axial compression load is imposed on the top surface of the imperfect shell, and the collapse load is obtained by using the explicit dynamic method. Increase the amplitude of perturbation loads until the collapsed load of the imperfect model converges. Third, the positions of multiple perturbation loads (including the axial and circumferential coordinates in cylindrical coordinates) are optimized to search for the low bound value of KDF. In this case, the perturbation load is 30 kN, and MIGA is used for the surrogate-based optimization.

Herein, lower bound KDF values of the Optimization V and the initial design are evaluated by means of WMPLA, and the obtained KDF values for Optimization V and the initial design are 0.72 and 0.69 respectively, which means the Optimization V has a lower imperfection sensitivity than the initial design. In addition, the KDF value for a traditional stiffened shell (with the same weight as the Optimization V) is predicted as 0.63 by WMPLA as mentioned in Ref. [2]. As demonstrated in Table 4, the Optimization V has the lowest KDF value, and thus it is less sensitive to imperfections and it can be considered as a robust and safe design. Above all, the optimal design obtained by the proposed optimization framework is verified to have a high buckling load and a low imperfection sensitivity.

4. Conclusion

In order to fully explore the optimal load-carrying efficiency of hierarchical stiffened shells, a bi-level optimization framework is proposed in this paper. In the first level, a parallel computing numerical-based smeared stiffener method (NSSM) is derived for the fast and explicit prediction of critical buckling load and mode. On the basis of NSSM, a large-scale Latin hypercube sampling (LHS) is performed among the entire design space, and then the Pareto front is collected as a set of competitive sampling points according to a screening criterion of load-carrying efficiency. After evaluating the critical buckling mode of competitive sampling results on the Pareto front, it indicates that the partial global buckling mode and global buckling mode are dominant buckling modes among all buckling modes of hierarchical stiffened shells, which contributes to achieving higher load-carrying efficiency. In the second level, an RBF surrogate model is established based on generated competitive sampling points. After that, a surrogate-based optimization is carried out to obtain the optimal collapse load. An illustrative example is performed to compare the computational efficiency and global optimizing ability between optimal results of the proposed method and the traditional surrogate-based optimization method. One interesting conclusion is that, when using the same

number of sampling points in surrogate models and an approximate total computational time, the optimal buckling result of the proposed method increases by 23.7% than that of the traditional method. Another conclusion is that, when searching out an approximate global optimization result, the proposed method can reduce the computational time sharply by 74.4% than the traditional method. Above all, the outstanding computational efficiency and global optimizing ability of the proposed method are validated. In addition, the low imperfection sensitivity of the optimal result is verified by means of WMPLA. The proposed bi-level optimization framework can be easily applied to other types of complicated shell structures, such as curvilinear stiffened shells, sandwich stiffened shells and corrugated shells. Furthermore, the SBPA or WMPLA would be integrated into the optimization framework of hierarchical stiffened shells, in order to consider the effect of imperfections on optimal designs and evaluate knockdown factors accurately.

Acknowledgements

This work was supported by National Basic Research Program of China [Grant no. 2014CB049000, No. 2014CB046506); National Natural Science Foundation of China (Grant no. 11372062, No. 11402049); Project funded by China Postdoctoral Science Foundation (Grant no. 2015T80246); 111 Project (Grant no. B14013). Kuo Tian appreciates the scholarship support from China Scholarship Council (Grant no. 201606060042).

References

[1] M. Yazdani, G. Rahimi, The effects of helical ribs' number and grid types on the buckling of thin-walled GFRP-stiffened shells under axial loading, J. Reinf. Plast. Compos. 29 (2010) 2568–2575.
[2] P. Hao, B. Wang, G. Li, Z. Meng, K. Tian, D. Zeng, X. Tang, Worst multiple perturbation load approach of stiffened shells with and without cutouts for improved knockdown factors, Thin-Walled Struct. 82 (2014) 321–330.
[3] F.F. Sun, H.L. Fan, C. Zhou, D.N. Fang, Equivalent analysis and failure prediction of quasi-isotropic composite sandwich cylinder with lattice core under uniaxial compression, Compos. Struct. 101 (2013) 180–190.
[4] P. Wang, F. Sun, H. Fan, W. Li, Y. Han, Retrofitting scheme and experimental research of severally damaged carbon fiber reinforced lattice-core sandwich cylinder, Aerosp. Sci. Technol. 50 (2016) 55–61.
[5] S. Jiang, F. Sun, H. Fan, Multi-failure theory of composite orthogrid sandwich cylinder, Aerosp. Sci. Technol. 70 (2017) 520–525.
[6] F.F. Sun, C.L. Lai, H.L. Fan, Failure mode maps for composite anisogrid lattice sandwich cylinders under fundamental loads, Compos. Sci. Technol. 152 (2017) 149–158.
[7] P. Hao, B. Wang, K. Tian, G. Li, K. Du, Y. Luan, Integrated optimization of hybrid-stiffness stiffened shells based on sub-panel elements, Thin-Walled Struct. 103 (2016) 171–182.
[8] D. Wang, M.M. Abdalla, Global and local buckling analysis of grid-stiffened composite panels, Compos. Struct. 119 (2015) 767–776.
[9] D. Quinn, A. Murphy, W. McEwan, F. Lemaitre, Stiffened panel stability behaviour and performance gains with plate prismatic sub-stiffening, Thin-Walled Struct. 47 (2009) 1457–1468.
[10] D. Quinn, A. Murphy, W. McEwan, F. Lemaitre, Non-prismatic sub-stiffening for stiffened panel plates–stability behaviour and performance gains, Thin-Walled Struct. 48 (2010) 401–413.
[11] D. Quinn, A. Murphy, C. Glazebrook, Aerospace stiffened panel initial sizing with novel skin sub-stiffening features, Int. J. Struct. Stab. Dyn. 12 (2012) 1250060.
[12] G. Houston, D. Quinn, A. Murphy, F. Bron, Design rules for stiffened panel buckling containment features, Thin-Walled Struct. 116 (2017) 69–81.
[13] B. Wang, P. Hao, G. Li, J.X. Zhang, K.F. Du, K. Tian, X.J. Wang, X.H. Tang, Optimum design of hierarchical stiffened shells for low imperfection sensitivity, Acta Mech. Sin. 30 (2014) 391–402.
[14] P. Hao, B. Wang, G. Li, Z. Meng, K. Tian, X.H. Tang, Hybrid optimization of hierarchical stiffened shells based on smeared stiffener method and finite element method, Thin-Walled Struct. 82 (2014) 46–54.
[15] B. Wang, K. Tian, C. Zhou, P. Hao, Y. Zheng, Y. Ma, J. Wang, Grid-pattern optimization framework of novel hierarchical stiffened shells allowing for imperfection sensitivity, Aerosp. Sci. Technol. 62 (2017) 114–121.
[16] Y.N. Zhao, M. Chen, F. Yang, L. Zhang, D.N. Fang, Optimal design of hierarchical grid-stiffened cylindrical shell structures based on linear buckling and nonlinear collapse analyses, Thin-Walled Struct. 119 (2017) 315–323.
[17] B. Wang, K. Tian, P. Hao, Y.W. Cai, Y.W. Li, Y. Sun, Hybrid analysis and optimization of hierarchical stiffened plates based on asymptotic homogenization method, Compos. Struct. 132 (2015) 136–147.
[18] B. Wang, K. Tian, H.X. Zhao, P. Hao, T.Y. Zhu, K. Zhang, Y.L. Ma, Multilevel optimization framework for hierarchical stiffened shells accelerated by adaptive equivalent strategy, Appl. Compos. Mater. 24 (2017) 575–592.
[19] F. Meng, B. Zhang, Z. Zhao, Y. Xu, H.L. Fan, F. Jin, A novel all-composite blast-resistant door structure with hierarchical stiffeners, Compos. Struct. 148 (2016) 113–126.
[20] C. Wang, Y. Xu, J. Du, Study on the thermal buckling and post-buckling of metallic sub-stiffening structure and its optimization, Mater. Struct. 49 (2016) 4867–4879.
[21] G. Rahimi, M. Zandi, S. Rasouli, Analysis of the effect of stiffener profile on buckling strength in composite isogrid stiffened shell under axial loading, Aerosp. Sci. Technol. 24 (2013) 198–203.
[22] P. Hao, B. Wang, G. Li, K. Tian, K. Du, X.J. Wang, X.H. Tang, Surrogate-based optimization of stiffened shells including load-carrying capacity and imperfection sensitivity, Thin-Walled Struct. 72 (2013) 164–174.
[23] B. Wang, K. Du, P. Hao, C.H. Zhou, K. Tian, S. Xu, Y.L. Ma, X. Zhang, Numerically and experimentally predicted knockdown factors for stiffened shells under axial compression, Thin-Walled Struct. 109 (2016) 13–24.
[24] B. Wang, S. Zhu, P. Hao, X. Bi, K. Du, B. Chen, X. Ma, Y.J. Chao, Buckling of quasi-perfect cylindrical shell under axial compression: a combined experimental and numerical investigation, Int. J. Solids Struct. 130–131 (2018) 232–247.
[25] S. Kidane, G. Li, J. Helms, S.-S. Pang, E. Woldesenbet, Buckling load analysis of grid stiffened composite cylinders, Compos. Part B-Eng. 34 (2003) 1–9.
[26] E. Wodesenbet, S. Kidane, S.-S. Pang, Optimization for buckling loads of grid stiffened composite panels, Compos. Struct. 60 (2003) 159–169.
[27] M. Buragohain, R. Velmurugan, Buckling analysis of composite hexagonal lattice cylindrical shell using smeared stiffener model, Def. Sci. J. 59 (2009) 230–238.
[28] B. Wang, P. Hao, G. Li, K. Tian, K. Du, X.J. Wang, X. Zhang, X.H. Tang, Two-stage size-layout optimization of axially compressed stiffened panels, Struct. Multidiscip. Optim. 50 (2014) 313–327.
[29] M.F. Ren, T. Li, Q.Z. Huang, B. Wang, Numerical investigation into the buckling behavior of advanced grid stiffened composite cylindrical shell, J. Reinf. Plast. Compos. 33 (2014) 1508–1519.
[30] T.M. Tu, P.H. Anh, N. Van Loi, T.A. Tuan, Optimization of stiffeners for maximum fundamental frequency of cross-ply laminated cylindrical panels using social group optimization and smeared stiffener method, Thin-Walled Struct. 120 (2017) 172–179.
[31] P.T. Thang, N.D. Duc, T. Nguyen-Thoi, Thermomechanical buckling and post-buckling of cylindrical shell with functionally graded coatings and reinforced by stringers, Aerosp. Sci. Technol. 66 (2017) 392–401.
[32] B. Wang, K. Tian, P. Hao, Y.B. Zheng, Y.L. Ma, J.B. Wang, Numerical-based smeared stiffener method for global buckling analysis of grid-stiffened composite cylindrical shells, Compos. Struct. 152 (2016) 807–815.
[33] Y.W. Cai, L. Xu, G.D. Cheng, Novel numerical implementation of asymptotic homogenization method for periodic plate structures, Int. J. Solids Struct. 51 (2014) 284–292.
[34] K. Tian, B. Wang, P. Hao, A.M. Waas, A high-fidelity approximate model for determining lower-bound buckling loads for stiffened shells, Int. J. Solids Struct. (2017), https://doi.org/10.1016/j.ijsolstr.2017.10.034.
[35] P. Hao, B. Wang, K. Tian, G. Li, Y. Sun, C.X. Zhou, Fast procedure for Non-uniform optimum design of stiffened shells under buckling constraint, Struct. Multidiscip. Optim. 55 (2017) 1503–1516.
[36] P. Hao, B. Wang, K. Tian, H.L. Liu, Y.T. Wang, F. Niu, D.J. Zeng, Simultaneous buckling design of stiffened shells with multiple cutouts, Eng. Optim. 49 (2017) 1116–1132.
[37] P. Hao, B. Wang, K. Tian, G. Li, K.F. Du, F. Niu, Efficient optimization of cylindrical stiffened shells with reinforced cutouts by curvilinear stiffeners, AIAA J. 54 (2016) 1350–1363.
[38] J.P. Peterson, P. Seide, V.I. Weingarten, Buckling of Thin-walled Circular Cylinders-NASA SP-8007. NASA Langley Research Center. Technical Report, (1968).
[39] B. Kriegesmann, R. Rolfes, C. Hühne, A. Kling, Fast probabilistic design procedure for axially compressed composite cylinders, Compos. Struct. 93 (2011) 3140–3149.
[40] M.W. Hilburger, A.E. Lovejoy, R.P. Thornburgh, C. Rankin, Design and analysis of sub- scale and full-scale buckling-critical cylinders for launch vehicle technology development, AIAA Paper 2012-1865, NF1676L-13285.
[41] M.W. Hilburger, W.T. Haynie, A.E. Lovejoy, M.G. Roberts, J.P. Norris, W.A. Waters, et al., Subscale and full-scale testing of buckling-critical launch vehicle shell structures, AIAA Paper 2012-1688, NF1676L-13284.
[42] H.N.R. Wagner, C. Hühne, S. Niemann, Robust knockdown factors for the design of axially loaded cylindrical and conical composite shells–Development and Validation, Compos. Struct. 173 (2017) 281–303.
[43] H.N.R. Wagner, C. Hühne, K. Rohwer, S. Niemann, M. Wiedemann, Stimulating the realistic worst case buckling scenario of axially compressed unstiffened cylindrical composite shells, Compos. Struct. 160 (2017) 1095–1104.
[44] H.N.R. Wagner, C. Hühne, S. Niemann, Constant single-buckle imperfection principle to determine a lower bound for the buckling load of unstiffened composite cylinders under axial compression, Compos. Struct. 139 (2016) 120–129.
[45] H.N.R. Wagner, C. Hühne, S. Niemann, R. Khakimova, Robust design criterion for axially loaded cylindrical shells-Simulation and validation, Thin-Walled Struct. 115 (2017) 154–162.
[46] H.N.R. Wagner, C. Hühne, Robust knockdown factors for the design of cylindrical shells under axial compression: potentials, practial application and reliability analysis, Int. J. Mech. Sci. 135 (2018) 410–430.
[47] H.N.R. Wagner, C. Hühne, S. Niemann, K. Tian, B. Wang, P. Hao, Design methods to determine knockdown factors for the buckling load of imperfection sensitive cylindrical shells under axial compression, Thin-Walled Struct. (2018).
[48] B. Wang, P. Hao, G. Li, Y.C. Fang, X.J. Wang, X. Zhang, Determination of realistic worst imperfection for cylindrical shells using surrogate model, Struct. Multidiscip.

Optim. 48 (2013) 777–794.
[49] G. Totaro, Z. Gürdal, Optimal design of composite lattice shell structures for aerospace applications, Aerosp. Sci. Technol. 13 (2009) 157–164.
[50] M. Bagheri, A. Jafari, M. Sadeghifar, A genetic algorithm optimization of ring-stiffened cylindrical shells for axial and radial buckling loads, Arch. Appl. Mech. 81 (2011) 1639–1649.
[51] A.H. Hashemian, M.H. Kargarnovin, J.E. Jam, Optimization of geometric parameters of latticed structures using genetic algorithm, Aircr. Eng. Aerosp. Technol. 83 (2011) 59–68.
[52] M. Abachizadeh, M. Tahani, An ant colony optimization approach to multi-objective optimal design of symmetric hybrid laminates for maximum fundamental frequency and minimum cost, Struct. Multidiscip. Optim. 37 (2009) 367–376.
[53] G. Venter, J. Sobieszczanski-Sobieski, Multidisciplinary optimization of a transport aircraft wing using particle swarm optimization, Struct. Multidiscip. Optim. 26 (2004) 121–131.
[54] K. Jarmai, J. Snyman, J. Farkas, Minimum cost design of a welded orthogonally stiffened cylindrical shell, Comput. Struct. 84 (2006) 787–797.
[55] A.R.M. Rao, K. Lakshmi, Optimal design of stiffened laminate composite cylinder using a hybrid SFL algorithm, J. Compos. Mater. 46 (2012) 3031–3055.
[56] F. Lene, G. Duvaut, M. Olivier-Mailhe, S.B. Chaabane, S. Grihon, An advanced methodology for optimum design of a composite stiffened cylinder, Compos. Struct. 91 (2009) 392–397.
[57] A. Khani, M. Abdalla, Z. Gürdal, Optimum tailoring of fibre-steered longitudinally stiffened cylinders, Compos. Struct. 122 (2015) 343–351.
[58] W. Liu, R. Butler, A.R. Mileham, A.J. Green, Bilevel optimization and postbuckling of highly strained composite stiffened panels, AIAA J. 44 (2006) 2562.
[59] S. DorMohammadi, M. Rais-Rohani, M. Rouhi, A multilevel approach for analysis and optimization of nano-enhanced composite structures, Compos. Struct. 131 (2015) 1050–1059.
[60] S. Shi, Z. Sun, M.F. Ren, H.R. Chen, X.Z. Hu, Buckling resistance of grid-stiffened carbon-fiber thin-shell structuresCompos. Pt. B-Eng, Compos. Part B-Eng. 45 (2013) 888–896.
[61] R.M. Jones, Mechanics of Composite Materials, Taylor & Francis, New York, 1999.
[62] M. Stein, Large sample properties of simulations using Latin hypercube sampling, Technometrics 29 (1987) 143–151.
[63] M.D. Shields, J.X. Zhang, The generalization of Latin hypercube sampling, Reliab. Eng. Syst. Saf. 148 (2016) 96–108.
[64] D. Whitley, S. Rana, R.B. Heckendorn, The island model genetic algorithm: on separability, population size and convergence, J. Comput. Inform. Technol. 7 (1999) 33–47.